frontiers | Frontiers in Energy Research

TYPE Original Research
PUBLISHED 28 March 2024
DOI 10.3389/fenrg.2024.1380501

OPEN ACCESS

EDITED BY
Minglei Bao,
Zhejiang University, China

REVIEWED BY
Zhenyu Zhou,
Waseda University, Japan
Sadia Umair,
National University of Computer and Emerging Sciences, Pakistan
Xiucai Ye,
University of Tsukuba, Japan

*CORRESPONDENCE
Zhan Shi,
w_1234567892021@163.com

RECEIVED 01 February 2024
ACCEPTED 06 March 2024
PUBLISHED 28 March 2024

CITATION
Shi Z (2024), Two-stage collaborative information interaction reliability improvement for the distribution grid. *Front. Energy Res.* 12:1380501. doi: 10.3389/fenrg.2024.1380501

Two-stage collaborative information interaction reliability improvement for the distribution grid

Zhan Shi*

Power Dispatching and Controlling Center of Guangdong Power Grid Company Limited, Guangzhou, China

The impulse noise generated by a large volume of power electronics devices imposes a hazardous impact on information interaction reliability in low-voltage distribution grids. In this paper, we propose a two-stage collaborative information interaction reliability improvement algorithm to minimize the bit error rate (BER) of the information interaction under impulse noise. In the first stage, the transmission-side peak-to-average power ratio (PAPR) is reduced based on the adaptive particle swarm optimization (PSO)-enabled partial transmit sequence (PTS). In the second stage, the reception-side dual-signal blanking is proposed based on the transmission-side PAPR and reception-side useful signal power estimation and peak median ratio. The transmission–reception collaborative information interaction reliability improvement is realized through two aspects. First, transmission-side PAPR reduction improves the performance of reception-side signal blanking by making it easier to distinguish useful signals from impulse noise. Second, the transmission-side PAPR is utilized to improve the estimation accuracy of both coarse and precise thresholds in dual-signal blanking. Simulation results show that the proposed algorithm outperforms existing algorithms in both PAPR reduction and BER performances to achieve information interaction reliability improvement effectively.

KEYWORDS

low-voltage distribution grid, information interaction, reliability improvement, dual-signal blanking, partial transmit sequence, particle swarm optimization

1 Introduction

Information interaction plays an important role in low-voltage distribution grid dispatch. As a widely used medium in low-voltage distribution grids, power line communication (PLC) has played a crucial role in realizing reliable information exchange. PLC takes existing power lines as the communication medium, which demonstrates the great advantages of low deployment costs, fast installation, and wide coverage (Yuwen et al., 2018; Khaled et al., 2018; Zhou et al., 2023). It can adapt well to the complex multi-branch and multi-load communication topology of low-voltage distribution grids (Antonio et al., 2015; Li et al., 2022a). However, with the large-scale integration of renewable energy resources, flexible loads, and energy storage units into distribution grids, the presence of a significant number of power electronics devices generates unignorable impulse noise, which significantly reduces

information interaction reliability and leads to the degradation of bit error rate (BER) performance (Nima et al., 2017; Ali et al., 2021a; Wen-Jing et al., 2022). How to ensure information interaction reliability for a low-voltage distribution grid under impulse noise remains an open issue (Tariq and Poor, 2018).

Impulse noise suppression is an important aspect of information interaction reliability improvement for low-voltage distribution grids, the core of which lies in the transmission-side peak-to-average power ratio (PAPR) reduction and reception-side signal blanking. On one hand, the adoption of orthogonal frequency division multiplexing (OFDM) (Bo et al., 2023; Liong et al., 2023) in PLC results in high transmission-side PAPR, which counteracts the effect of reception-side signal blanking because it is difficult to distinguish impulse noise from useful signals under high PAPR. A widely utilized approach to reducing the PAPR is the partial transmit sequence (PTS). It decomposes the original OFDM symbols into multiple subsequences and then performs weighting and phase modulation on each subsequence to achieve PAPR minimization. On the other hand, reception-side signal blanking suppresses impulse noise by nulling the signal whose amplitude is above a preset blanking threshold of zero. Its effectiveness in improving information interaction reliability of PLC has been proved due to its high feasibility and practicability in real-world applications (Wang et al., 2023).

However, although recent studies have achieved significant progress, the study on improving information interaction reliability in low-voltage distribution grids still faces some major technical challenges (Kelvin et al., 2017; Zhang et al., 2017). First, there is a lack of comprehensive consideration of transmission-side PAPR reduction and reception-side signal blanking from the perspective of collaboration (Gaëtan et al., 2008; Hongxiang and Tetsuya, 2016; Ali et al., 2021b). Information interaction reliability improvement is a complex problem that involves both the transmission and reception sides, and the transmission-side PAPR has an unignorable impact on reception-side signal blanking. Second, the selection of the optimal phase factor in the PTS has extremely high computational complexity. The search space of minimum PAPR increases exponentially with the number of partial sequences, and the simple utilization of the exhaustive method becomes infeasible (Satyendra Singh et al., 2015; Yassine and Abdelkrim, 2017; Li et al., 2023). Finally, signal blanking relying on a single threshold is less effective to deal with the scenario where low-amplitude impulse noise coexists with high-amplitude noise. The one-size-fits-all threshold tends to either suppress high-amplitude impulse noise but keep the low-amplitude one or even suppress both the impulse noise and useful signal, which has an adverse impact on information interaction reliability improvement (Filbert et al., 2016).

Numerous researchers have studied PTS for PAPR reduction. Sravanti and Vasantha (2017) proposed various precoding PTS methods to improve PAPR reduction performance based on the exhaustive method. Qian et al. (2019) proposed a PTS-based algorithm to search for the optimal phase factor using the exhaustive method, which reduces the PAPR of transmission signals. Zhang et al. (2020) proposed a permutated PTS scheme, which exhibits significantly higher PAPR reduction performance with less complexity by combining two operations of phase rotations and frequency-domain permutations. However, the above studies rely on exhaustive methods to search for the optimal phase factor, which is infeasible for practical implementation. The particle swarm optimization (PSO) algorithm can quickly find the optimal phase factor by simulating the interaction between particles. It has been widely applied to PTS due to the advantages of simultaneous utilization of both local and global information to improve the search performance. Ouqour et al. (2014) designed a PSO-based active constellation extension-projection onto convex sets (ACE-POCS) algorithm to reduce the PAPR of OFDM signals. However, the conventional PSO algorithm adopts a fixed inertial weight, which cannot be adaptively adjusted by the signal characteristic, leading to poor optimization accuracy and convergence speed. Moreover, the above studies do not consider signal blanking on the reception side. Nir and Ron (2014) proposed a narrowband noise suppression scheme based on frequency shift filtering, the objective of which is to improve the information exchange reliability of PLC. Gaëtan et al. (2010) investigated an impulse statistics estimation-based automatic noise mitigation algorithm to improve the BER performance of the information interaction. However, the above studies ignore the collaboration between the transmission-side PAPR and reception-side useful signal power estimation and peak median ratio, which cannot fully release the potential for impulse noise suppression. Furthermore, the mere consideration of a single-signal blanking threshold cannot achieve accurate impulse noise suppression.

To address these challenges, we propose a two-stage collaborative information interaction reliability improvement algorithm for low-voltage distribution grids. First, the transmission-side PAPR is reduced based on adaptive PSO-enabled PTS. Second, reception-side dual-signal blanking is proposed based on the transmission-side PAPR and reception-side useful signal power estimation and peak median ratio. Finally, through simulation results, we verify the effectiveness of the proposed algorithm in both PAPR reduction and BER performances. The main contributions of this work are summarized as follows:

- Two-stage collaborative impulse noise suppression for information interaction reliability improvement: the proposed algorithm realizes transmission–reception collaborative information interaction reliability improvement in two stages. In the first stage, the transmission-side PAPR is reduced by optimizing the phase factor of PST based on adaptive PSO, which improves the performance of reception-side signal blanking by making it easier to distinguish useful signals from impulse noise. In the second stage, the transmission-side PAPR is further used to calculate both coarse and precise thresholds, which can effectively improve the blanking threshold accuracy based on signal characteristics.
- Transmission-side PAPR reduction based on the adaptive PSO-enabled PTS: we propose a transmission-side PAPR reduction based on the adaptive PSO-enabled PTS to preprocess the frequency domain signal. By dynamically adjusting the adaptive inertia weight of PSO based on differentiated PAPRs, the proposed algorithm can adaptively adjust the global and local search capabilities. Global search is adopted to improve the searching speed under large PAPR, while local search is adopted to improve the searching accuracy under small PAPR. In this way, the proposed algorithm can avoid falling into the local optimum and improve the search precision.

- Reception-side dual-signal blanking based on useful signal power estimation and peak median ratio: we propose reception-side dual-signal blanking based on the transmission-side PAPR and reception-side useful signal power estimation and peak median ratio. The proposed algorithm uses the transmission-side PAPR to carry out coarse blanking, which blanks high-amplitude impulse noise to improve useful signal power estimation for precise signal blanking. Then, precise signal blanking is carried out based on useful signal power estimation and the peak median ratio. The precise threshold is set to approach the peak value of the useful signal so that the low-amplitude impulse noise can be precisely suppressed.

The remainder of this paper is organized as follows: Section 2 formulates the system model. The proposed adaptive PSO and dual blanking-based two-stage collaborative information interaction reliability improvement algorithm is presented in Section 3. The simulation results are provided in Section 4. Finally, conclusions are drawn in Section 5.

2 System model

PLC is a complex process, including transmission and reception, and the whole communication process consists of many aspects. During the information interaction of PLC, impulse noise is generated by a large number of power electronics devices, which will seriously affect the quality of PLC and lead to data transmission errors and even transmission interruptions. Compared with modulation methods such as code division, multiple access, and time division multiplexing, OFDM divides the signal into multiple subcarriers, limiting the impact of impulse noise (Wang et al., 2019). Furthermore, by dynamically adjusting the power distribution of subcarriers, OFDM reduces the effect of impulse noise on the entire PLC communication system (Hou et al., 2023). In order to reduce the impact of impulse noise on PLC, it is necessary to establish a complete OFDM signal transmission model to lay the foundation for information interaction reliability improvement.

2.1 Signal transmission model

The complete OFDM signal transmission model is shown in Figure 1. At the transmitter, the binary bit data are modulated as a frequency domain signal by Q-phase shift keying (QPSK). $\mathbf{A}$ is defined as the original frequency domain signal, which is given by Eq. (1)

$$\mathbf{A} = [A_1, A_2, \ldots, A_n, \ldots, A_N]^{\mathrm{T}}, \tag{1}$$

where N is the number of subcarriers and $\mathbf{A}_N$ represents the data carried by the Nth subcarrier.

PTS is a phase optimization scheme that works by splitting the original signal into multiple sub-sequences and weighting these sub-sequences using different phase factors. Then, the weighted sub-sequences are superimposed together before transmission. It effectively reduces the high PAPR generated by OFDM modulation and improves the interaction reliability performance of the signal. We divide N subcarriers into L disjoint subsets, each of which contains M subcarriers, i.e., $N = L \times M$. For each subset, M corresponding subcarriers are selected from the original frequency domain signal to form a partial sequence. The set of partial sequences is defined as $\Omega = \{Q_1, Q_2, \ldots, Q_l, \ldots, Q_L\}$, where $\mathbf{Q_l}$ is the partial sequence of the lth subset and represented as Eq. (2)

$$\mathbf{Q}_l = \left[A_{q_1}, \ldots, A_{q_m}, \ldots, A_{q_M}\right]^{\mathrm{T}}, \tag{2}$$

where $q_1, \ldots, q_m, \ldots, q_M$ are the indexes of the selected subcarriers in the subset.

PAPR, the peak-to-average power ratio of a signal, is used as a measure of the dynamic range and complexity of a signal. A lower PAPR indicates a higher resolution between the noise generated during signal transmission and the useful signal, which improves the information interaction reliability performance. By weighting partial sequences, the phase can be adjusted to avoid high PAPR in the process of signal superposition. Therefore, the phase factor $b_l = \exp(j\varphi_l)$ is introduced as the auxiliary information to weigh partial sequences, where $\varphi_l \in [0, 2\pi)$. By choosing different phase factors to weigh partial sequences, the generated integrated discrete time domain signal x_k is given by Eq. (3)

$$\begin{aligned} x_k &= \sum_{l=1}^{L} \mathrm{IDFT}\{b_l \mathbf{Q}_l)\} \\ &= \sum_{l=1}^{L} b_l \mathrm{IDFT}\{\mathbf{Q}_l\} \\ &= \sum_{l=1}^{L} b_l \mathbf{q}_l, k = 1, \ldots, N, \end{aligned} \tag{3}$$

where $\mathbf{q}_1$ is the discrete time-domain signal of $\mathbf{Q}_1$. The PAPR of x_k is represented as Eq. (4)

$$\mathrm{PAPR}(x_k) = 10\lg\left(\frac{\max\limits_{k=1,2,\ldots,N} |x_k|^2}{\frac{1}{N}\sum\limits_{k=1}^{N} |x_k|^2}\right). \tag{4}$$

In order to obtain the time-domain signal with the lowest PAPR, it is necessary to choose the optimal phase factor sequence, which is given by Eq. (5)

$$\{b_1, b_2, \ldots, b_l\} = \arg\min_{\{b_1, b_2, \ldots, b_l\}} \left(\max_{1 \le k \le N} |x_k|^2\right), \tag{5}$$

where $\arg\min\{\cdot\}$ denotes the value of the independent variable when the function reaches its minimum value. In order to better describe the reduction degree of the signal PAPR before and after the weighted integration of phase factors, we adopt the complementary cumulative distribution function (CCDF) to characterize the degree of reduction in the PAPR, which is given by Eq. (6)

$$\mathrm{CCDF}(x_k) = \Pr\left(\mathrm{PAPR}(x_k) > \mathrm{PAPR}^*\right), \tag{6}$$

where $\mathrm{PAPR}*$ is the threshold of the transmission-side PAPR.

2.2 Noise model

According to Antoniali et al. (2016), during the information interaction of PLC, the relevant research mainly classifies the noise

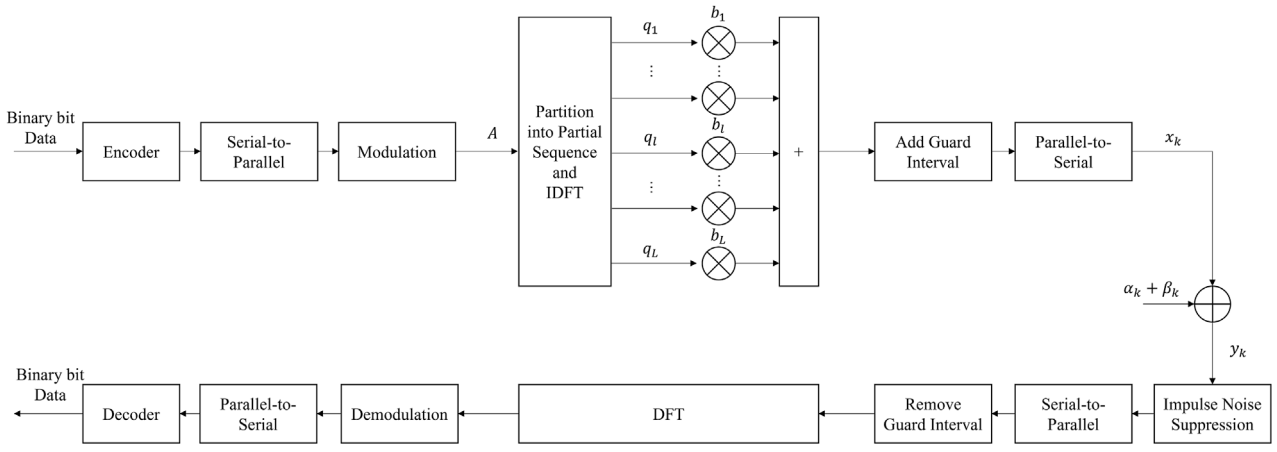

FIGURE 1
Complete OFDM signal transmission model.

into two categories, i.e., background noise and impulse noise, according to the variation in noise and the amplitude of fluctuation over time. Background noise varies more smoothly in a certain time range, with little amplitude fluctuation and a long duration. Impulse noise is mainly caused by the sudden switching of the working state of high-power electronic equipment and contains multiple frequency components in the frequency domain (Tariq et al., 2020; Li et al., 2022b). It covers a wide frequency range and has a high impact on the quality of PLC. The Middleton class A noise model is used to model PLC impulse noise (Savoia and Verde, 2013). The overall noise is given by Eq. (7)

$$\omega_k = \alpha_k + \beta_k, \quad k = 1, \ldots, N, \tag{7}$$

where α_k is the background noise of the tth OFDM symbol period and can be expressed as additive Gaussian white noise. β_k is the impulse noise, which can be described as the multiplication of Gaussian noise and a Bernoulli process (Axell et al., 2015), in Eq. (8),

$$\beta_k = \mu_k g_k, \tag{8}$$

where g_k is the zero-mean white Gaussian noise and μ_k is the Bernoulli process. The probability density function of μ_k is expressed as Eq. (9)

$$f_\mu(\mu_k) = \begin{cases} \lambda, & \mu_k = 1 \\ 1-\lambda, & \mu_k = 0, \end{cases} \tag{9}$$

where $\mu_k = 1$ indicates the presence of impulse noise and $\mu_k = 0$ indicates the absence of impulse noise. λ is the probability of generating impulse noise. The noise probability density function over a period of time can be obtained, which is given by Eq. (10)

$$\begin{aligned} f_\omega(\omega_k) = (1-\lambda)\, G\left(\omega_k, 0, \sigma_\alpha^2\right) \\ + \lambda G\left(\omega_k, 0, \sigma_\alpha^2 + \sigma_\beta^2\right), \end{aligned} \tag{10}$$

where σ_α^2 is the variance in background noise, σ_β^2 is the variance in the impulse noise, and $G(\cdot)$ is the Gaussian probability density function.

2.3 Bit error rate model

According to the description of the noise model, the total noise in the channel of the OFDM system is composed of additive white Gaussian noise and impulse noise. The power spectral densities of additive Gaussian white noise and impulse noise are defined as N_α and N_β, respectively (Abdo et al., 2018). We use QPSK to modulate the transmission-side signal of the OFDM system. The BER under noise is expressed as Eq. (11)

$$\mathrm{BER} = Q\left(\sqrt{\frac{2E_b}{N_\alpha + N_\beta}}\right), \tag{11}$$

where E_b is the binary code energy of the OFDM signal. $Q(\cdot)$ is the right tail function of the standard normal distribution, which is given by Eq. (12)

$$Q(z) = \int_z^\infty \frac{1}{2\pi} e^{-\frac{t^2}{2}} dt = \frac{1}{2}\mathrm{erfc}\left(\frac{z}{\sqrt{2}}\right). \tag{12}$$

3 Adaptive PSO and dual blanking-based two-stage collaborative information interaction reliability improvement for low-voltage distribution grids

In this section, we propose an adaptive PSO and dual blanking-based two-stage collaborative information interaction reliability improvement algorithm for low-voltage distribution grids. Specifically, in the first stage, we endeavor to reduce the transmission-side PAPR by optimizing the phase coefficients of the PST, thereby enhancing the resolution between the impulse noise and the useful signal. Subsequently, in the second stage, we utilize the decreased transmission-side PAPR from the first stage to compute coarse and precise thresholds, thereby elevating the blanking performance of the reception-side signal in the second phase. Ultimately, this approach achieves transmission–reception

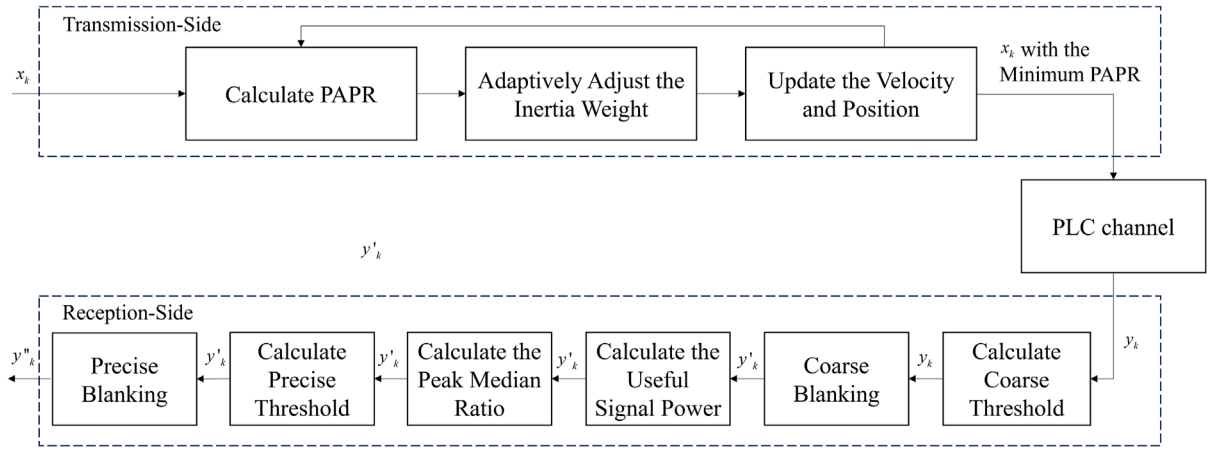

FIGURE 2
Overall structure of the proposed algorithm.

collaborative information interaction reliability improvement. Without the collaboration of the two stages, the PAPR on the transmission side may not effectively decrease, thereby affecting the performance of impulse noise suppression. In the first stage, we successfully reduce the transmission-side PAPR by optimizing phase coefficients, enhancing the resolution between impulse noise and useful signals. The second stage utilizes the reduced transmission-side PAPR to calculate coarse and precise thresholds, further improving the blanking performance of the reception-side signal. Neglecting the collaboration in the second stage could result in a reduced resolution between impulse noise and useful signals, inaccurate threshold calculations, and, consequently, an impact on the impulse noise suppression performance. The proposed algorithm is shown in Algorithm 1. The overall structure of the proposed algorithm is shown in Figure 2.

3.1 First-stage transmission-side PAPR reduction based on the adaptive PSO-enabled PTS

The traditional PTS algorithm has high complexity since it needs to search for the optimal phase factors using the exhaustive method. The PSO algorithm realizes PTS optimization by simulating the interaction between particles to effectively reduce computational complexity.

PSO designs massless particles to simulate the individuals in a swarm. The particle contains two attributes defined as velocity s and position p, where s reflects the moving speed of the particles in the swarm and p reflects the moving direction of the particles. The particles' positions indicate potential solutions, while their speeds determine the direction and speed of movement within the search space. Integrating speed and position attributes with the article's specific content can enhance the algorithm's problem-specific nature, thereby increasing the search efficiency and accuracy. The optimal solution searched by each particle individually is denoted as the current individual optimal value v^{ind} and shared with other particles in the swarm. The optimal solution searched by all particles in the swarm is denoted as the current global optimal value v^{glo}. The optimal solution is the one with the best performance based on the fitness function value in the current iteration cycle. The individual optimal value is the best solution found in each particle's history. The global optimal value is the best solution found in the history of all particles in the entire particle swarm. By comparing these values, the optimal solution in the current iteration cycle may evolve into the individual optimal solution and potentially evolve into the global optimal solution.

We consider G iterations, the set of which is $\mathcal{G} = \{1, \ldots, g, \ldots, G\}$. After the optimal solution is searched in the gth iteration, PSO updates the position and velocity of the particle based on its inertial, cognitive, and social components to adjust the search direction and step size in the $(g+1)$th iteration. The position $p_i(g+1)$ and velocity $s_i(g+1)$ of the ith particle in the $(g+1)$th iteration are updated as Eq. (13) and Eq. (14) (Fernandez-Martinez and Garcia-Gonzalo, 2011; Anamika et al., 2018):

$$s_i(g+1) = \theta s_i(g) + l_1 r_1 \left(v_i^{\mathrm{ind}}(g) - p_i(g)\right) + l_2 r_2 \left(v^{\mathrm{glo}}(g) - p_i(g)\right), \tag{13}$$

$$p_i(g+1) = p_i(g) + s_i(g+1), \tag{14}$$

where r_1 and r_2 are the random numbers within [0,1]. θ is the inertia weight factor, which serves to balance the local and global search ability of PSO. l_1 and l_2 are the learning factors, which reflect the tendency of each particle to search toward itself or the swarm. $v_i^{\mathrm{ind}}(g)$ and $v^{\mathrm{glo}}(g)$ are the individual optimal value of the ith particle and global optimal value in the gth iteration, respectively. $\theta s_i(g)$ is the inertia part, which reflects the motion behavior of the particle, i.e., the tendency of the particle to maintain its previous state. $l_1 r_1 \left(v_i^{\mathrm{ind}}(g) - p_i(g)\right)$ is the cognitive part, which reflects the particle's memory of its own historical experience and represents the particle's tendency to approach its historical optimal position. $l_2 r_2 \left(v^{\mathrm{glo}}(g) - p_i(g)\right)$ is the social part, which reflects the swarm history experience on cooperation and knowledge sharing among the particles and represents the tendency of the particles to approach the best position in the swarm history.

Input: G, s, l_1, l_2, s_{max}, A, b_1, L, N, C, M, h, p, σ_α, σ_β, θ_{ini}, θ_{end}, r_1, and r_2.
Stage 1: First-stage transmission-side PAPR reduction algorithm based on the adaptive PSO-enabled PTS
Initialize s, p, l_1, l_2, G, s_{max}, N^{ph}, L, N, θ_{ini}, θ_{end}, r_1, and r_2.
For $g = 1:G$ **do**
Divide the original frequency domain signal into L partial sequences and weigh the above partial sequences by different phase factors according to the PTS.
Calculate the minimum $PAPR(x_k)$ and use it as a fitness function.
Obtain v^{ind} and v^{glo} based on the fitness function.
Adaptively adjust the inertia weight according to (17).
Update the particle velocity and position based on (16) and (18).
Determine whether s exceeds the maximum speed limit s_{max}.
If $g = G$
Output v^{glo}. The final v^{glo} is the minimum $PAPR(x_k)$.
else
$g = g + 1$.
End if
End for
Stage 2: Second-stage reception-side dual-Signal blanking based on **the transmission-side PAPR and reception-side useful signal power estimation and peak median ratio**
Coarse blanking based on the transmission-side PAPR:
Calculate the coarse threshold Γ of the signal amplitude based on (19).
Perform coarse blanking based on (20).
Precise blanking based on reception-side useful signal power estimation and peak median ratio:
Calculate the difference between the average power of the original reception-side signal and the average power after coarse suppression based on (21).
Calculate the useful signal power based on (22).
Calculate the parameters ϖ and ξ based on the peak and median values of the reception-side signal.
Calculate the precise threshold $\Gamma*$ of the signal amplitude based on ϖ, ξ, and the useful signal power.
Perform precise blanking based on (26).
End

Algorithm 1. Adaptive PSO and dual blanking-based two-stage collaborative information interaction reliability improvement for low-voltage distribution grids.

In actual OFDM systems, the phase factor is generally selected from a specific set to reduce computation complexity, which is presented as Eq. (15)

$$b_l \in \left\{ \exp j2\pi \left[\frac{[0{:}N^{ph}-1]}{N^{ph}} \right] \right\}, \tag{15}$$

where N^{ph} is the number of phase factors.

However, the traditional PSO algorithm has the problems of slow convergence speed and poor optimization accuracy. To address these challenges, we propose a first-stage transmission-side PAPR reduction algorithm based on the adaptive PSO-enabled PTS. It adopts PSO to quickly find the optimal phase factors of PTS and uses PAPR of the transmission-side signal to dynamically adjust the weights of local and global search, improving the speed and accuracy of PSO.

Based on the traditional PSO algorithm, $s_{i,d}(g)$ is defined as the velocity of the dth dimension of the ith particle in the gth iteration, which is updated as

$$\begin{aligned} s_{i,d}(g+1) = {} & \theta(g)\, s_{i,d}(g) + l_1 r_1 \left(v_i^{\mathrm{ind}}(g) \right) - p_{i,d}(g) \big) + \\ & l_2 r_2 \left(v^{\mathrm{glo}}(g) \right) - p_{i,d}(g) \big), \end{aligned} \tag{16}$$

where $\theta(g)$ is the adaptive inertia weight. $\theta(g)$ is calculated as

$$\theta(g) = \mathrm{PAPR}(x_k) * \frac{(\theta_{\mathrm{ini}} - \theta_{\mathrm{end}})(G-g)}{G} + \theta_{\mathrm{end}}, \tag{17}$$

where θ_{ini} is the initial inertia weight and θ_{end} is the inertia weight in the Gth iteration. The adaptive inertia weight decreases with an increase in the number of iterations, and the local search ability is increased to make the algorithm converge faster. At the same time, when $\mathrm{PAPR}(x_k)$ is larger, it tends to perform the global search as a way to expand all positions and reduce the PAPR as quickly as possible. When $\mathrm{PAPR}(x_k)$ is smaller, it tends to maintain its previous state and refine the exploration of local positions to approach the optimal solution faster. Through (17), the global and local search capabilities can be adaptively adjusted based on the transmission-side PAPR and provide better convergence performance to effectively reduce the algorithm complexity of the PTS method.

$p_{i,d}(g)$ is defined as the position of the dth dimension of the ith particle in the gth iteration, which is updated as

$$p_{i,d}(g+1) = \begin{cases} 1, & \mathrm{rand!sig}\left(s_{i,d}(g+1)\right) \\ 0, & \mathrm{else}, \end{cases} \tag{18}$$

where $\mathrm{sig}(s_{i,d}(g+1)) = \frac{1}{1+\exp(s_{i,d}(g+1))}$.

Thus, the implementation steps of the first-stage transmission-side PAPR reduction algorithm based on the adaptive PSO-enabled PTS are as follows:

1) N_p particle swarms are randomly generated in a $N^{ph} * L$ dimensional space. Learning factors l_1 and l_2, position p, velocity s, maximum speed limit s_{max}, maximum number of iterations G, the number of phase factors N^{ph}, disjoint subset number L, subcarrier number in a disjoint subset M, and subcarrier number N are initialized.
2) Based on the PTS method, the original frequency domain signal is divided into L partial sequences, which are multiplied by different phase factors after IDFT.

3) The minimum $PAPR(x_k)$ of the transmission-side signal x_k is calculated and used as a fitness function. The search values v^{ind} and v^{glo} are obtained according to the fitness function.
4) Based on $PAPR(x_k)$, $\theta(g)$ is adaptively adjusted according to (17). The velocity and position of the particles are updated based on (16, 18). Whether s exceeds the maximum speed limit $s_{\max}$ is determined.
5) The iterative process of learning is repeated until the maximum number of iterations G is reached. The final v^{glo} is the minimum $\mathrm{PAPR}(x_k)$.

3.2 Second-stage reception-side dual-signal blanking based on the transmission-side PAPR and reception-side useful signal power estimation and the peak median ratio

The proposed algorithm involves two parts: the transmission side and reception side. The proposed algorithm is conducted in two stages. After PAPR reduction at the transmission side is completed, the second stage of the proposed algorithm occurs. In the second stage, the reception-side signal is blanked to improve information interaction reliability by suppressing impulse noise. Traditional single-blanking-based impulse noise suppression algorithms realize impulse noise suppression by zeroing out the impulse noise with a preset threshold. Due to the influence of parameter uncertainty and the characteristics of the signal, the preset threshold is not precise, which makes it difficult to suppress the impulse noise through the threshold. Therefore, we propose a second-stage reception-side dual-signal blanking based on the transmission-side PAPR and reception-side useful signal power estimation and peak median ratio, which consists of coarse and precise blanking and can be applied to all low-voltage distribution network systems. Dual blanking refers to the proposed algorithm performing two-step blankings, i.e., the first one being coarse blanking followed by precise blanking. Impulse noise suppression can be effectively realized by these two-step blankings. Replacing single-signal banking with the proposed dual-signal blanking will increase the additional calculation cost, but the calculation of dual-signal blanking is simple and the added cost is minimal. Moreover, dual-signal blanking can significantly enhance the impulse noise suppression capability. The detailed steps of this algorithm are shown as follows.

3.2.1 Coarse blanking based on the transmission-side PAPR

The coarse threshold Γ of the signal amplitude is calculated by combining the PAPR of the transmission-side signal, which is given by

$$\Gamma = \sqrt{\mathrm{PAPR}(x_k) \times \frac{1}{N}\sum_{k=1}^{N}|y_k|^2}, \tag{19}$$

where y_k represents the reception-side signal and $\frac{1}{N}\sum_{k=1}^{N}|y_k|^2$ represents the average reception-side signal power. Γ should be located between the maximum signal envelope without noise and the maximum waveform of the reception-side envelope. In the first stage, the signal with lower PAPR is obtained based on the adaptive PSO-enabled PTS, which indicates that the dynamic range of the useful signal is small and the amplitude gap with the impulse noise amplitude is large. Therefore, we perform coarse filtering of the reception-side signal according to this feature in the coarse blanking stage, thus realizing the cooperative impulse noise suppression at the transmission side and reception side.

According to Γ, a coarse blanking method is used to suppress impulse noise, which is given by

$$y'_k = \begin{cases} y_k & ,if|y_k| \le C\Gamma \\ 0 & ,if|y_k| > C\Gamma, \end{cases} \tag{20}$$

where C represents the coarse estimation threshold adjustment factor. It can adjust Γ to avoid the elimination of useful signals. Through the above processing, the impulse noise greater than $C\Gamma$ is suppressed.

3.2.2 Precise blanking based on the reception-side useful signal power estimation and peak median ratio

Based on the coarse blanking results of the reception-side signal y'_k, the difference between the average power of the original reception-side signal and the average power after coarse blanking can be given by

$$D = \frac{1}{N}\sum_{k=1}^{N}\left(|y_k|^2 - |y'_k|^2\right). \tag{21}$$

The impulse noise power suppressed in the coarse blanking can be approximated as D, but the actual impulse noise power is larger than D. We introduce the constant τ to adjust D so that the estimated average power is closer to the actual useful signal power, which ensures that the obtained threshold is more accurate. Useful signal power R is given by

$$R = \frac{1}{N}\sum_{k=1}^{N}|y_k|^2 - \tau D \times \frac{\sum_{k=1}^{N}|y'_k|^2}{\sum_{k=1}^{N}|y_k|^2}, \tag{22}$$

where $\frac{\sum_{k=1}^{N}|y'_k|^2}{\sum_{k=1}^{N}|y_k|^2}$ is the ratio of the average power of the received signal after coarse blanking to the average power of the received signal before coarse blanking.

Then, the peak value of the useful signal can be obtained using the transmission signal PAPR and useful signal power. To improve the blanking accuracy, we adjust the threshold based on the peak median ratio of the received signal in the precise blanking to realize precise noise suppression.

The parameters ϖ and ξ are calculated based on the peak and median values of the received signal. ξ is the peak median ratio of the received signal. The concepts of peak median ratio and PAPR are distinct as they delineate different aspects of a signal in the time domain. Specifically, PAPR quantifies the discrepancy between the peak power and the average power of a signal. A higher PAPR indicates a greater disparity between the peak and average

powers, potentially leading to signal distortion and degraded system performance. On the other hand, the peak median ratio represents the difference between the peak power and the median power of a signal. In contrast to the PAPR, the peak median ratio is typically employed to characterize signal stability and waveform symmetry. The parameters ϖ and ξ are given by Eq. (23) and Eq. (24)

$$\varpi = \frac{\underset{k=1,2,\ldots,N}{\text{median}}\left(|y_k|\right)}{\eta}, 0 < \eta < 1, \tag{23}$$

$$\xi = \sqrt{\frac{\underset{k=1,2,\ldots,N}{\max}\left(|y_k|\right)}{\underset{k=1,2,\ldots,N}{\text{median}}\left(|y_k|\right)}}, \tag{24}$$

where η is a constant used to adjust the parameter calculation and median(·) represents the median function.

Useful signal power and the peak median ratio are combined to calculate the precise threshold $\Gamma*$ of the signal amplitude, which is given by Eq. (25)

$$\Gamma^* = (1-h)\sqrt{\text{PAPR}(x_k)\times R} + h\frac{\varpi\times\sqrt{2\log(N)}}{1+\sqrt{1+\frac{\xi}{2}}}, \tag{25}$$

where h represents the balance parameter and $\frac{\varpi\times\sqrt{2\log(N)}}{1+\sqrt{1+\frac{\xi}{2}}}$ is the threshold based on parameters. Due to the reduction in the useful signal's PAPR at the transmitter and the high power characteristics of impulse noise, the value of parameter ξ is larger. A larger parameter ξ brings $\Gamma*$ closer to the peak of the useful signal, thus suppressing low-amplitude impulse noise.

According to $\Gamma*$, precise blanking is carried out to improve the blanking accuracy of impulse noise, which is given by

$$y_k'' = \begin{cases} y_k' & ,if|y_k'| \le \Gamma^* \\ 0 & ,if|y_k'| > \Gamma^*. \end{cases} \tag{26}$$

4 Simulation results

In this section, we evaluate the information interaction reliability improvement performance of the proposed algorithm through simulation. The simulation is implemented through MATLAB. We consider an OFDM communication system with 256 subcarriers using QPSK modulation. Other detailed simulation parameters are shown in Table 1 (Emad and Khaled, 2013; Khaled and Emad, 2014).

Two state-of-the-art algorithms are used for comparison. The first algorithm is dynamic peak-based threshold estimation (DPTE), which improves information interaction reliability by analyzing the relationship between the optimal blanking threshold and the peak value of OFDM symbols and using the peak amplitude of the OFDM symbol as the noise suppression threshold (Khaled and Emad, 2014). The second is the dynamic peak-based threshold estimation–partial transmission sequence (DPTE-PTS), which considers PTS-based PAPR reduction before implementing DPTE and realizes PTS optimization by conventional PSO (Khaled and Emad, 2014).

TABLE 1 Simulation parameters.

Parameter	Value	Parameter	Value
N	256	M	8
L	2, 4, 8, 16, and 32	N^{ph}	4
l_1	2	l_2	2
Q3-4: s_{max}	0.2	G	250
θ_{ini}	0.9	θ_{end}	0.4
h	0.5		

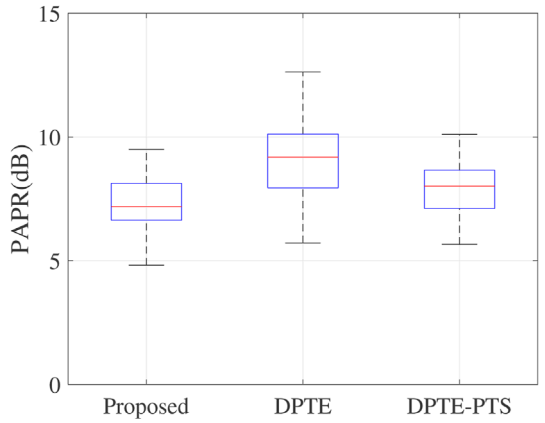

FIGURE 3
Q2-5: Transmission-side PAPR fluctuation under different algorithms.

The complexity of the proposed algorithm includes two stages. In the first stage, the computational complexity of PSO depends on the number of particles and the number of iterations and can be calculated as $\mathcal{O}(3I\times G)$, where I represents the total number of particles. In the second stage, computational complexity simply depends on the number of mathematical calculations, and the computational complexity is $\mathcal{O}(8)$. It is worth mentioning that the complexity of using single-signal blanking in the second stage is $\mathcal{O}(2)$. Therefore, the computational complexity of the proposed algorithm is $\mathcal{O}(3I\times G+8)$. The computational complexity of DPTE is $\mathcal{O}(3G)$. DPTE-PTS also adopts the PSO algorithm, and its computational complexity is $\mathcal{O}(3(I+1)\times G)$. Since DPTE does not consider PAPR reduction on the transmission side, its computational complexity is less, but the impulse noise suppression performance of DPTE is poor.

Figure 3 shows the box plot of the transmission-side PAPR, illustrating the fluctuation of the transmission-side PAPR under different algorithms. Compared with DPTE and DPTE-PTS, the proposed algorithm has the smallest PAPR fluctuation and reduces the average PAPR by 24.7% and 16.1%, respectively. The reason is that the proposed algorithm optimizes phase factor selection for PST through adaptive PSO to improve the PAPR reduction

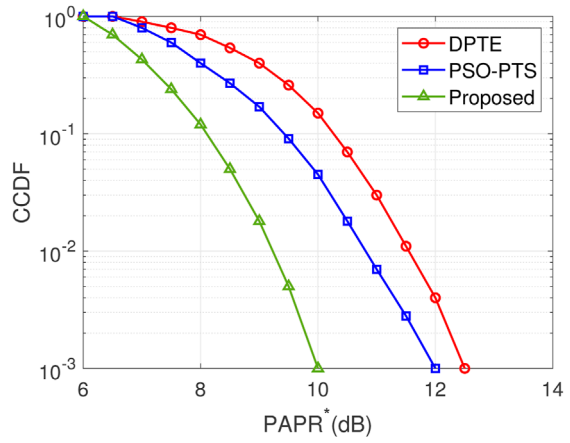

FIGURE 4
CCDF of PAPR reduction under different algorithms.

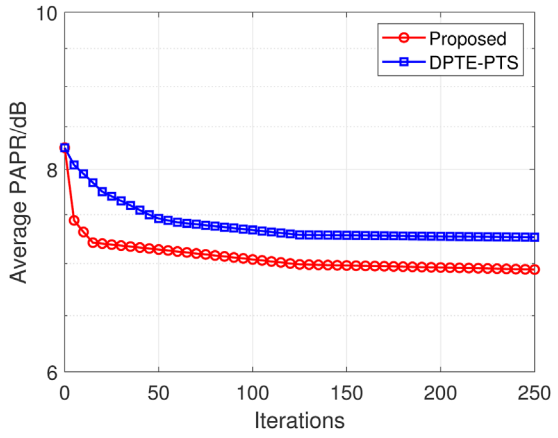

FIGURE 6
Average PAPR versus PSO iterations.

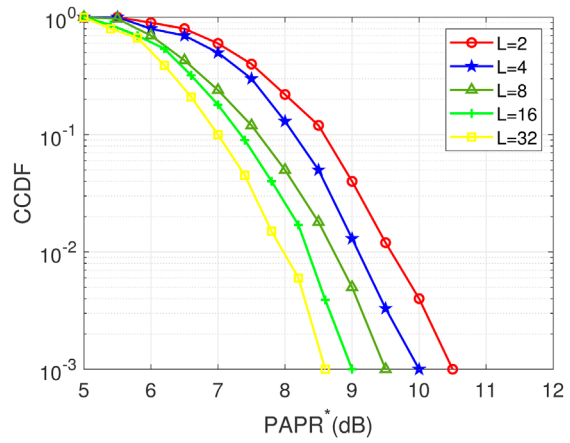

FIGURE 5
CCDF of PAPR reduction of the proposed algorithm under different *L* values.

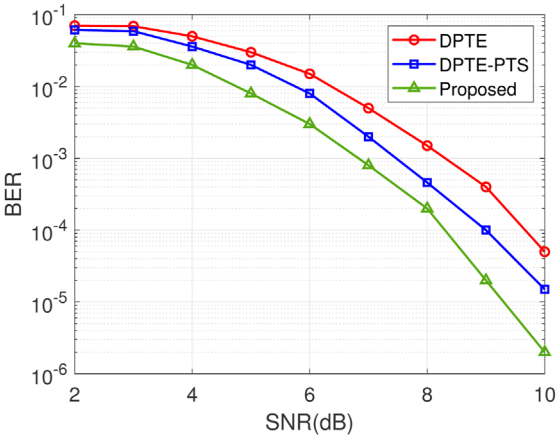

FIGURE 7
BER performance versus SNR.

performance. Simultaneously, it utilizes the PAPR to adaptively update inertia weights based on signal characteristics so as to balance between global search and local search, leading to better convergence performance, higher searching accuracy, and smaller PAPR fluctuation. DPTE neglects selection optimization of phase factors for PTS, which leads to higher transmission-side PAPR. DPTE-PTS cannot adaptively adjust its search strategy according to the change in PAPR, resulting in a slower searching speed and poor search accuracy.

Figure 4 shows the CCDF of PAPR reduction under different algorithms. Compared with DPTE and DPTE-PTS, the proposed algorithm can realize better PAPR reduction performance. The reason is that the proposed algorithm uses the PAPR to realize the dynamic adjustment of the inertia weight of PSO, thus effectively improving the search accuracy and PAPR performance. In this way, the probability that the transmission-side PAPR exceeds the PAPR threshold is effectively reduced.

Figure 5 shows the CCDF of PAPR reduction with different L values. The proposed algorithm decomposes the original OFDM symbols into L subsequences and then performs weighting and phase modulation on each subsequence to reduce the PAPR of the signal at the transmission side. As L increases, more phase factors are utilized to weigh the decomposed partial subsequences, achieving better PAPR reduction. However, the computational complexity also increases exponentially with L.

Figure 6 shows the average PAPR versus PSO iterations. As the number of PSO iterations increases, the average PAPR of the proposed algorithm first decreases and finally stabilizes after $g = 25$, while that of DPTE-PTS also decreases at first and finally stabilizes after $g = 50$. When $g = 250$, compared with DPTE-PTS, the proposed algorithm reduces the average PAPR by 4.5%. The reason is that the proposed algorithm dynamically adjusts the updating of inertia

weights based on PAPR variation. It combines global search under large PAPR and local search under small PAPR to jointly improve the convergence rate and searching accuracy of PSO.

Figure 7 shows the variation in the BER versus SNR. Since data transmission involves the interaction between the transmission side and the reception side, the higher the interaction reliability between the transmission and reception sides, the smaller the BER of the reception-side signal. Therefore, the BER can reflect the interaction reliability of the proposed algorithm. When SNR = 10 dB, the BER of the proposed algorithm decreases by 81.3% and 65% compared with DPTE and DPTE-PTS, respectively. The reason is that the proposed algorithm achieves two-stage collaborative information interaction reliability improvement by suppressing the impulse noise. The first stage uses adaptive PSO to optimize PTS to reduce transmission-side PAPR, which improves the amplitude gap between impulse noise and the useful signal. The second stage utilizes reception-side dual-signal blanking to further suppress the impulse noise. DPTE does not consider PTS or transmission-side PAPR reduction. The signal blanking effectiveness is counteracted due to the degraded resolution between the useful signal and impulse noise, thereby resulting in higher BER. DPTE-PTS performs better than DPTE because it considers PTS-enabled transmission-side PAPR reduction to improve reception-side signal blanking. However, its performance is worse than the proposed algorithm because it cannot adaptively adjust inertia weight updating, according to PAPR variation, and the searching of the phase factor is prone to being trapped in local optimum. Furthermore, it does not consider the combination of coarse and precise blanking so that impulse noise whose amplitude is close to that of a useful signal cannot be accurately identified and suppressed.

5 Conclusion

In this paper, we addressed the problem of insufficient reliability of information interaction for low-voltage distribution grids under impulse noise caused by the high proportion of power electronics devices and proposed a two-stage collaborative information interaction reliability improvement algorithm for low-voltage distribution grids. Compared with DPTE and DPTE-PTS, the average PAPR of the proposed algorithm is reduced by 65.5% and 34.5%, and the BER of the proposed algorithm decreases by 81.3% and 65% when $SNR = 10$ dB. This demonstrates that the collaboration between transmission-side PAPR reduction and reception-side signal blanking has obvious performance gains. We have provided insights into combining PTS and signal blanking to improve information interaction reliability, but the form of collaboration is not constrained by PTS and signal blanking. Meanwhile, the proposed work is still applicable in the case of SINR. However, the proposed method does not consider the effect of background noise or the frequency domain characteristics of impulse noise. In the future, considering the coupling of noise features in the time and frequency domains, we will further look into information interaction reliability improvement based on historical performance feedback from a reinforcement learning perspective.

Data availability statement

The raw data supporting the conclusion of this article will be made available by the authors, without undue reservation.

Author contributions

ZS: writing–review and editing and writing–original draft.

Funding

The author(s) declare that financial support was received for the research, authorship, and/or publication of this article. This work was supported by the Science and Technology Project of China Southern Power Grid Corporation under the grant number 036000KK52220020 (GDKJXM20220276).

Conflict of interest

Author ZS was employed by Power Dispatching and Controlling Center of Guangdong Power Grid Company Limited.

The authors declare that this study received funding from Science and Technology Project of China Southern Power Grid Corporation. The funder had the following involvement in the study: collection, analysis, interpretation of data, the writing of this article, and the decision to submit it for publication.

Publisher's note

All claims expressed in this article are solely those of the authors and do not necessarily represent those of their affiliated organizations, or those of the publisher, the editors, and the reviewers. Any product that may be evaluated in this article, or claim that may be made by its manufacturer, is not guaranteed or endorsed by the publisher.

References

Abdo, A. M. A., Zhao, X., Zhang, R., Zhou, Z., Zhang, J., Zhang, Y., et al. (2018). MU-MIMO downlink capacity analysis and optimum code weight vector design for 5G big data massive antenna millimeter wave communication. *IEEE J. Sel. Areas Commun.* 2018, 1–12. doi:10.1155/2018/7138232

Ali, F. T., Hen-Geul, Y., and Seok-Chul, K. (2021a). BER performance of space–time parallel ICI cancellation of OFDM in MIMO power line communications. *IEEE Syst. J.* 15 (2), 1742–1752. doi:10.1109/jsyst.2020.2968542

Ali, M., Adnan, M., Tariq, M., and Poor, H. V. (2021b). Load forecasting through estimated parametrized based fuzzy inference system in smart grids. *IEEE Trans. Fuzzy Syst.* 29 (1), 156–165. doi:10.1109/tfuzz.2020.2986982

Anamika, Peesapati, R., and Kumar, N. (2018). Electricity price forecasting and classification through wavelet–dynamic weighted PSO–FFNN approach. *IEEE Syst. J.* 12 (4), 3075–3084. doi:10.1109/jsyst.2017.2717446

Antoniali, M., Versolatto, F., and Tonello, A. M. (2016). An experimental characterization of the PLC noise at the source. *IEEE Trans. Power Deliv.* 31 (3), 1068–1075. doi:10.1109/tpwrd.2015.2452939

Antonio, C., Giovanni, C., Valentina, C., Cara, D. D., Dio, V. D., Guaiana, S., et al. (2015). A prototypal architecture of a IEEE 21451 network for smart grid applications based on power line communications. *IEEE Sensors J.* 15 (5), 2460–2467. doi:10.1109/jsen.2014.2336377

Axell, E., Wiklundh, K. C., and Stenumgaard, P. F. (2015). Optimal power allocation for parallel two-state Gaussian mixture impulse noise channels. *IEEE Wirel. Commun. Lett.* 4 (2), 177–180. doi:10.1109/lwc.2015.2388759

Bo, Y., Bao, M., Ding, Y., and Hu, Y. (2023). A DNN-based reliability evaluation method for multi-state series-parallel systems considering semi-Markov process. *Reliab. Eng. Syst. Saf.* 242, 109604. doi:10.1016/j.ress.2023.109604

Emad, A., and Khaled, R. (2013). "Dynamic peak-based threshold estimation method for mitigating impulsive noise in power-line communication systems," in IEEE Transactions on Power Delivery (IEEE), 2201-2208. doi:10.1109/TPWRD.2013.2272766

Fernandez-Martinez, J. L., and Garcia-Gonzalo, E. (2011). Stochastic stability analysis of the linear continuous and discrete PSO models. *IEEE Trans. Evol. Comput.* 15 (3), 405–423. doi:10.1109/tevc.2010.2053935

Filbert, H. J., Qinghua, G., Yifan, C., Xu, L., Huang, D. D., and Wong, K. P. (2016). Linear combining of nonlinear preprocessors for OFDM-based power-line communications. *IEEE Trans. Smart Grid* 7 (1), 253–260. doi:10.1109/tsg.2015.2403953

Gaëtan, N., Pierre, S., and Marie-Hélène, H. (2008). Optimization of turbo decoding performance in the presence of impulsive noise using soft limitation at the receiver side. *IEEE Glob. Telecommun. Conf.*, 1–5.

Gaëtan, N., Pierre, S., and Marie-Hélène, H. (2010). Adaptive noise mitigation in impulsive environment: application to power-line communications. *IEEE Trans. Power Deliv.* 25 (2), 647–656. doi:10.1109/tpwrd.2009.2035505

Hongxiang, C., and Tetsuya, S. (2016). A new PTS method for OFDM signals without side information based on constellation reshaping. *Annu. Conf. Inf. Sci. Syst. (CISS)*, 216–221.

Hou, Y., Bao, M., Sang, M., and Ding, Y. (2023). A market framework to exploit the multi-energy operating reserve of smart energy hubs in the integrated electricity-gas systems. *Appl. Energy* 357, 122279. doi:10.1016/j.apenergy.2023.122279

Kelvin, A., Bamidele, A., Khaled, R., Hammoudeh, M., and Gacanin, H. (2017). On companding and optimization of OFDM signals for mitigating impulsive noise in power-line communication systems. *IEEE Access* 5, 21818–21830. doi:10.1109/access.2017.2747629

Khaled, R., Bamidele, A., Haris, G., and Yarkan, S. (2018). Energy-per-bit performance analysis of relay-assisted power line communication systems. *IEEE Trans. Green Commun. Netw.* 2 (2), 360–368. doi:10.1109/tgcn.2018.2794613

Khaled, R., and Emad, A. (2014). "On enhancing the performance of the DPTE-based noise cancellation method utilizing the PTS PAPR reduction scheme in PLC systems," in 18th IEEE International Symposium on Power Line Communications and Its Applications, 334–339.

Li, Z., Wu, L., Xu, Y., Moazeni, S., and Tang, Z. (2022a). Multi-stage real-time operation of a multi-energy microgrid with electrical and thermal energy storage assets: a data-driven MPC-ADP approach. *IEEE Trans. Smart Grid* 13 (1), 213–226. doi:10.1109/tsg.2021.3119972

Li, Z., Wu, L., Xu, Y., and Zheng, X. (2022b). Stochastic-weighted robust optimization based bilayer operation of a multi-energy building microgrid considering practical thermal loads and battery degradation. *IEEE Trans. Sustain. Energy* 13 (2), 668–682. doi:10.1109/tste.2021.3126776

Li, Z., Xu, Y., Wang, P., and Xiao, G. (2023). Restoration of multi energy distribution systems with joint district network recon figuration by a distributed stochastic programming approach. *IEEE Trans. Smart Grid*, 1. doi:10.1109/tsg.2023.3317780

Liong, A. A. G., Gopal, L., Rong, Y., Juwono, F. H., and Chiong, C. W. R. (2023). Power optimization of a three-node two-way relay-assisted power-line communication system. *IEEE Trans. Power Deliv.* 38 (1), 200–211. doi:10.1109/tpwrd.2022.3181297

Nima, T., Lutz, L., and Shahriar, M. (2017). An adaptive impedance-matching system for vehicular power line communication. *IEEE Trans. Veh. Technol.* 66 (2), 927–940. doi:10.1109/tvt.2016.2562629

Nir, S., and Ron, D. (2014). Frequency-shift filtering for OFDM signal recovery in narrowband power line communications. *IEEE Trans. Commun.* 62 (4), 1283–1295. doi:10.1109/tcomm.2014.020514.130421

Ouqour, A., Jabrane, Y., Said, B. A. E., and Ouahman, A. A. (2014). PAPR reduction in OFDM via active constellation extension–projection onto convex sets combined with particle swarm optimization. *Comput. J.* 57 (8), 1230–1237. doi:10.1093/comjnl/bxt073

Qian, Y., Zhou, X., Li, J., Shu, F., and Jayakody, D. N. K. (2019). A novel precoding and impulsive noise mitigation scheme for MIMO power line communication systems. *IEEE Syst. J.* 13 (1), 6–17. doi:10.1109/jsyst.2018.2880962

Satyendra Singh, Y., Prasanta Kumar, P., and Sarat Kumar, P. (2015). "Computational complexity analysis of PTS technique under graphics processing unit," in Proceedings of the 2015 Third International Conference on Computer, 1–5.

Savoia, R., and Verde, F. (2013). Performance analysis of distributed space–time block coding schemes in Middleton class-A noise. *IEEE Trans. Veh. Technol.* 62 (6), 2579–2595. doi:10.1109/tvt.2013.2240396

Sravanti, T., and Vasantha, N. (2017). "Precoding PTS scheme for PAPR reduction in OFDM," in 2017 International Conference on Innovations in Electrical, Electronics, Instrumentation and Media Technology (United States: ICEEIMT), 250–254.

Tariq, M., Adnan, M., Srivastava, G., and Poor, H. V. (2020). Instability detection and prevention in smart grids under asymmetric faults. *IEEE Trans. Industry Appl.* 56 (4), 1–4520. doi:10.1109/tia.2020.2964594

Tariq, M., and Poor, H. V. (2018). Electricity theft detection and localization in grid-tied microgrids. *IEEE Trans. Smart Grid* 9 (3), 1–1929. doi:10.1109/tsg.2016.2602660

Wang, X., Umehira, M., Akimoto, M., Han, B., and Zhou, H. (2023). Green spectrum sharing framework in B5G era by exploiting crowdsensing. *IEEE Trans. Green Commun. Netw.* 7 (2), 916–927. doi:10.1109/tgcn.2022.3186282

Wang, Y., He, Y., Xu, C., Zhou, Z., Mumtaz, S., Rodriguez, J., et al. (2019). Joint rate control and power allocation for low-latency reliable D2D-based relay network. *J. Wirel. Commun. Netw.* 2019, 111. doi:10.1186/s13638-019-1418-0

Wen-Jing, L., Nan, Z., Zhu, L., Wang, J. F., Guo, Y. S., and Lv, D. (2022). Information fusion method of power internet of things based on low-voltage power line and micro-power wireless communication. *IEEE Access* 10, 89959–89969. doi:10.1109/access.2022.3201514

Yassine, H., and Abdelkrim, B. (2017). Robust image transmission over powerline channel with impulse noise. *Multimedia Tools Appl.* 76 (2), 2813–2835. doi:10.1007/s11042-015-3216-y

Yuwen, Q., Jun, L., and Yijin, Z. (2018). Performance analysis of an opportunistic relaying power line communication systems. *IEEE Syst. J.* 12 (4), 3865–38685.

Zhang, D., Zhou, Z., Xu, C., Zhang, Y., Rodriguez, J., and Sato, T. (2017). Capacity analysis of NOMA with mmwave massive MIMO systems. *IEEE J. Sel. Areas Commun.* 35 (7), 1606–1618. doi:10.1109/jsac.2017.2699059

Zhang, W., Gao, X., Li, Z., and Shi, Y. (2020). Pilot-assisted MIMO-V-OFDM systems: compressed sensing and deep learning approaches. *IEEE Access* 8, 7142–7159. doi:10.1109/access.2020.2964046

Zhou, H., Wang, X., Umehira, M., Han, B., and Zhou, H. (2023). *Energy efficient beamforming for small cell systems: a distributed learning and multicell coordination approach*. ACM Transactions on Sensor Networks.